Macromolecular Research

Article

DOI 10.1007/s13233-022-0089-6

www.springer.com/13233 pISSN 1598-5032 eISSN 2092-7673

Structure and Properties of Low Dielectric Constant Polyetherimide Films Containing-CF_3 and Cardo Groups

Jun Peng[1,3]
Qian Wang[3]
Jin Wang[3]
Jun Yang[3]
Taijun Jiang*[,4]
Guangsheng Zeng*[,1,2]

[1] School of Urban and Environmental Science, Hunan University of Technology, Zhuzhou 412007, P. R. China
[2] College of Electromechanical Engineering, Changsha University, Changsha 410022, P. R. China
[3] Zhuzhou Times New Material Technology Co. Ltd, Zhuzhou 412007, P. R. China
[4] Intelligent Manufacturing Institute, Hunan Railway Professional Technology College, Zhuzhou 412001, P. R. China

Received May 17, 2022 / Revised June 11, 2022 / Accepted June 19, 2022

Abstract: Cardo containing phenoxy and -CF_3 derivate diamine was synthesized, and further it was polymerized with 3,3',4,4'-biphenyl tetracarboxylic dianhydride to prepare polyetherimide containing Cardo group. The transmittance of the prepared polymer increased from 82% to 88% and the dielectric constant decreased from 2.91 to 2.83 with a slight decline in thermal and mechanical performance when -CF_3 was introduced. The molecular simulation in terms of charge distribution, electric potential energy, chain stiffness and aggregation state revealed that -CF_3 could restrain charge transfer and decrease the unit dipole moment and polarization for its larger volume. The optical and dielectric performance was significantly enhanced, but the thermal and mechanical performance decreased slightly when the -CF_3 group was introduced. The glass transition temperature of the polymer declined from 329 ℃ to 311 ℃. The investigation conducted in this paper can offer valuable reference to the optimization and development of synthesis and comprehensive performance of polyimide.

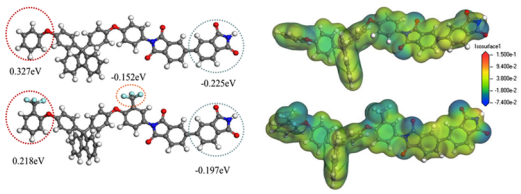

Keywords: cardo group, polyetherimide, micro-structure, dielectric constant.

1. Introduction

The demand for polymers of low dielectric and dielectric loss, such as liquid crystal polymer (LCP) and polyphenylene sulfide (PPS), has experienced continuously increase in recent years with the rapid development of electronic appliance and 5G equipment.[1,2] Polyimide (PI) turned out to be the best candidate for its excellent chemical resistance, heat stability and mechanical performance,[3,4] but the extensively existed charge transfer effect would result in the deficiency in optical property and dielectric loss.[5] Many researchers have been devoted to the design and fabrication of PI film.[6,7]

As a biphenyl structure of rigidity cardo group could be easily modified in structure, and diversified derivatives could be prepared by introducing different functional groups.[8] Functional monomer could be obtained by introducing additional group or making certain modification on the active group in cardo group. In addition to excellent solubility and transparency, Cardo-based PI has outstanding thermal stability and dielectric properties.[9-11] And it can be widely used in separating membrane[12,13] and exchange membrane.[14] Spirofluorene-Cardo group has attracted many researchers[15] and the larger side group can give us more features.[16,17] Cardo group is a fluorophore,[18] and high-performance luminescence film can be prepared by introducing fluorene group in PI chains.[19,20] More and more attention has been paid to the development of PI containing cardo group.

Molecular simulation approach was used to promote the exploration and development of PI from the perspectives of energy,[21] geometry[22] and morphology.[23] To find out the critical factors concerning comprehensive performance of PI many researchers have carried out lot of simulations to investigate the effect of filling state, configuration, aggregation state, hydrogen-bond interaction, crystalline degree and modulus on the performance of PI materials.[24-27]

The modified cardo group was introduced into polyimide skeleton to prepare monomer, and later polyetherimide was synthesized with existence of 3,3',4,4'-biphenyl tetracarboxylic dianhydride (BPDA) as dianhydride.[28,29] The microstructural, mechanical, thermal, optical and dielectric property was characterized and investigated. To explore the relationship between microstructure and performance of the material the density function theory and molecular dynamic was used to simulate the interaction between chain segments, especially for the macro effect of -CF_3 group in the presence of large side cardo group.

Acknowledgments: This work was sponsored by national natural science foundation of China under grant 51973056 and 52173034, Hunan provincial project of science and technology under grant 2020NK2035, 2021JJ50031 and 2021JJ50009, scientific research projects of Hunan provincial department of education under grant 18A258 and 18C0524, the science and technology innovation program of Hunan province under grant 2021RC4065.

***Corresponding Authors:** Taijun Jiang (jiangtaijun@126.com), Guangsheng Zeng (guangsheng_zeng@163.com)

2. Experimental

2.1. Materials

9,9-Bis(4-hydroxyphenyl) fluoren, hydrazine monohydrate, p-chloronitrobenzene, 1-chloro-4-nitro-2-(trifluoromethyl) benzene, potassiumcar bonate and palladium on activated charcoal was purchased from Alfa-Aesar. 3,3',4,4'-Biphenyl tetracarboxylic dianhydride (BPDA) was purchased from Mitsubishi Chemical (Japan). *N*-Methyl pyrrolidone (NMP) was produced by BASF. Other analytical grade reagents and solvents were purchased from National Pharmaceutical Group Chemical Reagent Co., Ltd. All regents and solvents were used without further purification.

2.2. Preparation of diamine

The synthetic scheme of 4,4'-(((9H-fluorene-9,9-diyl)bis(4,1-phenylene))bis(oxy))dianiline (Cardo-AP) and 4,4'-(((9H-fluorene-9,9-diyl)bis(4,1-phenylene))bis(oxy))bis(3-(trifluoromethyl)aniline) (Cardo-FA) was illustrated in Scheme 1.

Cardo-NO_2: 10.0 mmol 9,9-bis(4-hydroxyphenyl) fluoren, 21.0 mmol p-chloronitrobenzene (or 1-chloro-4-nitro-2-(trifluoromethyl) benzene), 21.5 mmol potassium carbonate and 50 mL NMP was filled into three-necked flask with condensing reflux unit and magnetic stirrer and heated to 120 ℃ in oil bath under reflux conditions for 12 h. Inorganic potassium was removed and the crude product was obtained after suction filtration and water washing. The crude product was further washed with alcohol and dried at 60 ℃ to get the faint yellow powder.

Cardo-NH_2: 0.02 mol Cardo-NO_2 and 350 ml absolute ethyl alcohol was filled into 500 ml three-necked flask and stirred in argon atmosphere. The homogenous suspension was later heated to 80 ℃ and afterward 0.05 g Pd/C (10 %wt) was added. 8 mL hydrazine hydrate was dropwise added under reflux conditions for 24 h. Palladium on carbon was removed after suction filtration from the reaction mixture, the filtrate was then poured into ethyl alcohol and was frozen at the temperature of -18 ℃ to form needle-like sample. The Cardo-NH_2 was obtained as the needle-like samples was dried at 80 ℃ after suction filtration.

Cardo-AP: FT-IR (KBr, V, cm^{-1}): 3476/3380 (amine N-H stretching), 3036 (aromatic ring, C-H), 1620 (NH_2, deformation), 1495 (1,4-phenylene), 1237/1168 (C-O-C). Figure S3.

^{1}H NMR (400 MHz, DMSO-d6, ppm): 7.87 (d, 2H), 7.37 (m, 4H), 7.27 (t, 2H), 6.99 (d, 4H), 6.71–6.65 (m, 8H), 6.55 (d, 4H, J = 8.8 Hz), 4.96 (s, 4H). Figure 1.

MS (EI, m/z): 532 ([M]+, calcd for $C_{37}H_{28}N_2O_2$, 532.64). Figure S5. Melting point (DSC): 238 ℃. Figure S4.

Cardo-FA: FT-IR (KBr, V, cm^{-1}): 3480/3375 (amine N-H), 3025 (Aromatic ring, C-H), 1618 (NH_2, deformation), 1493 (1,4-phenylene), 1233/1170 (C-O-C), 1050/1338 (-CF_3). Figure S3.

^{1}H NMR (400 MHz, DMSO-d6, ppm): 7.88 (d, 2H), 7.37 (m, 4H), 7.28 (t, 2H), 6.98 (d, 4H), 6.69 (m, 6H), 6.51 (d, 4H), 4.96 (s, 4H). Figure 1.

MS (EI, m/z): 668 ([M]+, calcd for $C_{39}H_{26}F_6N_2O_2$, 668.64). Figure S6. Melting point (DSC): 175 ℃. Figure S3.

2.3. Preparation of PEI

BPDA was polymerized with above prepared diamine, as listed in Scheme 2. 0.04 mol Cardo-NH_2 and NMP (solid content wt/wt 15%) was added into a three-necked flask at the temperature of 20 ℃ under mechanical stirring. 0.04 mol BPDA was added into the mixture in batches in a decreasing manner of 60%, 30%, 5%, 3%, 1%, *et al.*, respectively every hour after the Cardo-NH_2 was completely dissolved. Finally, adjusted the amount of BPDA according to the viscosity. The viscosity of PAA was measured in 1 h after 0.002 g BPDA was added into the solution. Stop the reaction until the objective viscosity was reached. To eliminate the influence of subsequent tests as a result of decreased -CF_3 reactivity the viscosity of the slurry was fixed at a 100 ± 10 Pa·s in the end.

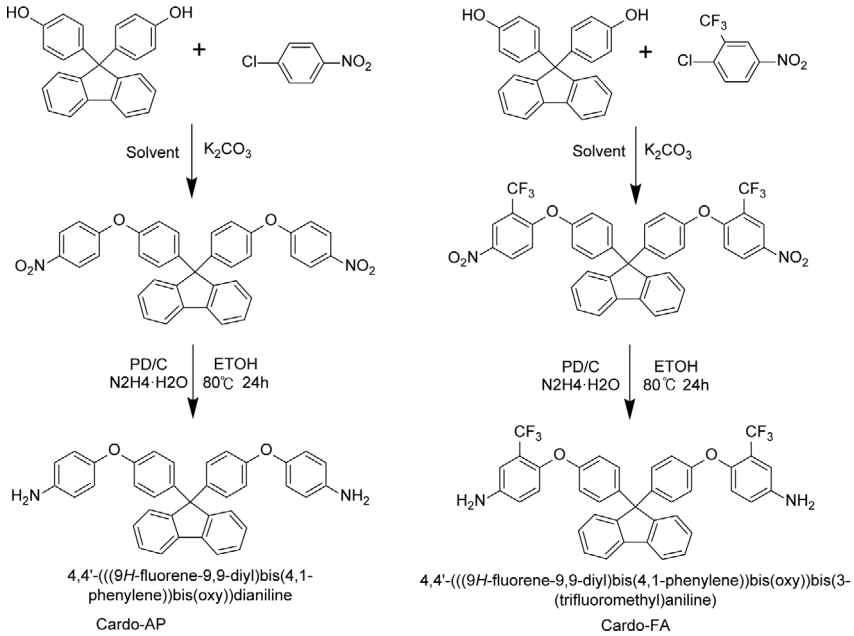

Scheme 1. Synthetic process of Cardo-NH_2.

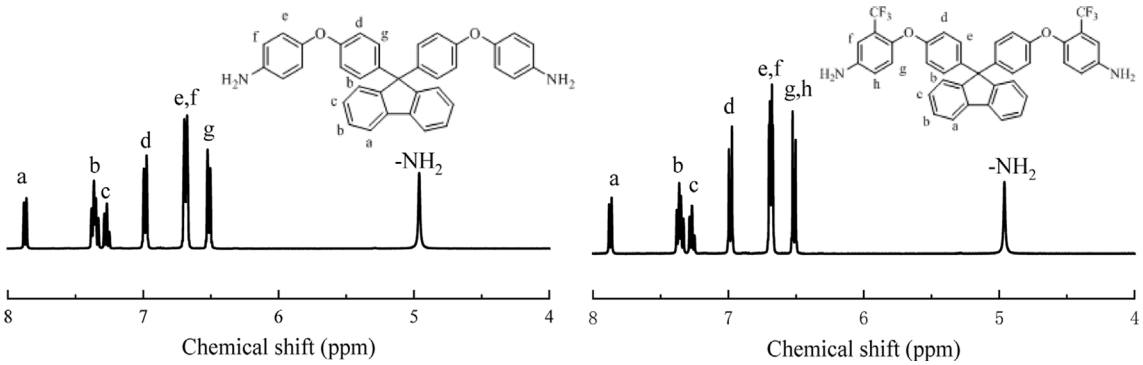

Figure 1. The ^{1}H-NMR spectra of the Cardo-AP and Cardo-FA.

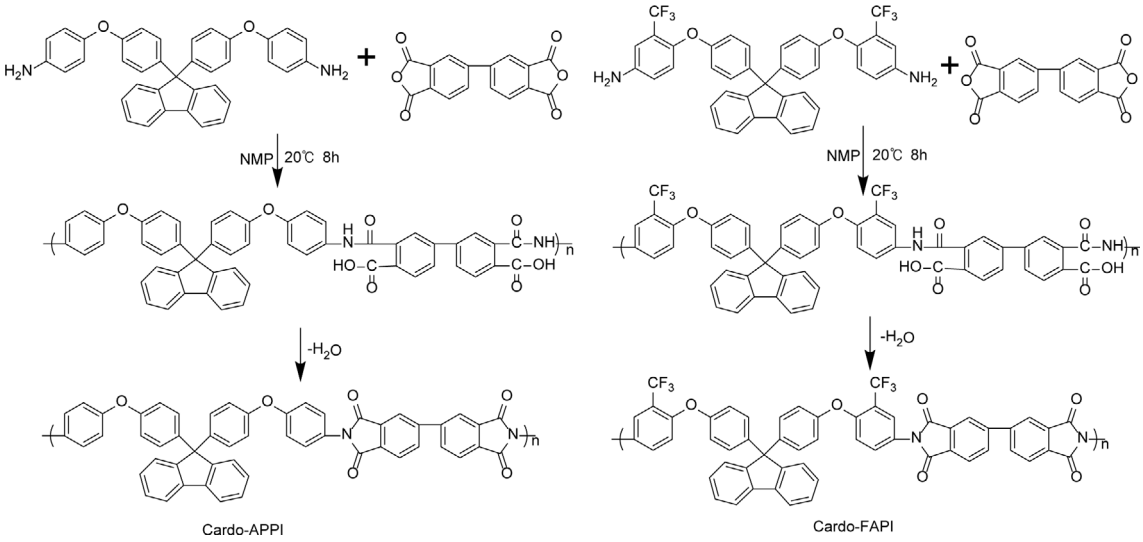

Scheme 2. Synthetic process of PEIs.

The slurry was firstly degassed in vacuum and then evenly coated on a glass plate with a scraper of 150 μm. Then, the thermal imidization was taken place by cyclodehydration of the PAA film by sequential heating (1 h at 100 ℃, 1 h at 200 ℃, 1 h at 300 ℃, 1 h at 350 ℃). Finally, the film was peeled off from the glass plate. Polyimide prepared *via* abovementioned Scheme 2 was indicated by Cardo-APPI and Cardo-FAPI.

2.4. Characterization

Nuclear magnetic resonance spectra (^{1}H NMR) was performed on a Bruker AVANCE AV 400 spectrometer.

Wide angle X-ray diffraction (WAXD) measurements were conducted to characterize the aggregation structure of polyimide film on Ultima IV XRD diffractometer (Rigaku, Japan) with Cu radiation and at 40 kV and 30 mA. The diffraction patterns were collected over 5-60° with a scanning speed of 8°/min.

The density of PEI films was measured by a density balance (Mirage SD-200 L, Japan) with an accuracy of 0.1 mg.

FT-IR spectra was obtained from Fourier-transform infrared (PerkinElmer, USA) spectrometer to characterize the chemical structure. Thermogravimetric analysis (TGA) was performed on TGA/DSC 1/1100 (METTLER TOLEDO, Switzerland) in nitrogen atmosphere at a heating rate of 10 ℃/min. Dynamic mechanical analysis (DMA) was conducted on DMA 242E (NETZSCH, USA). The heating rate and frequency was 5.0 ℃/min and 1 Hz respectively. CTE of the film was measured with thermomechanical analysis Q400 (TA USA) in tension mode. The tension force and heating rate was set to 0.02 N and 5 ℃/min. The temperature range was set to 50-400 ℃. The optical properties of the films were characterized by a UV spectrophotometer. the thickness of the films was fixed at 15 μm and the test wavelength covered 800 nm to 200 nm. Dielectric constant and dielectric loss (tanδ) of films were measured by a precision impedance analyzer (Agilent 4294A) with platinum electrode (1 cm × 1 cm). The measurements were conducted at room temperature within the frequencies from 10^{3} Hz to 10^{7} Hz.

2.5. Molecular simulation

Materials Studio 8.0 from Accelrys was used to simulate molecular dynamics for a better understanding of the structural differences at molecular level.

Repeat units and polymer chains of Cardo-PI, Cardo-APPI and Cardo-FAPI was constructed. 25 repeat units were used and amino group was taken as the initiator and terminator. Ten polymer chains were employed for the amorphous cell construction. Isotactic polymer configuration with random torsion and head-to-tail orientation was assumed for the simulation. The amorphous cell module was used to construct a polymeric

periodic cell based on COMPASS forcefield calculations at temperature of 298 K and reduced densities of 0.2 g/cm^3 to simulate the dense polyimide. The geometry of the configuration could be optimized by the construction of the amorphous cell.[30] The optimized cells were compressed with isothermal-isobaric (NPT) ensemble dynamics at the pressures of 0.001 GPa and a dynamics time of 1,000 ps. The system was afterward relaxed *via* a series of anneal dynamics and stage wise equilibration procedure. The anneal dynamics contains 10 anneal cycles from 300 K to 1,000 K with 14 heating ramps per cycle. Next, the systems were dynamically equilibrated in NPT and canonical (NVT) ensemble at the temperature of 298 K. We set the step time and dynamics time to be 1.0 fs and 500 ps respectively.[31-34]

The free volume and occupied volume of polyimides could be calculated by Eq. (1).

$$FFV = \frac{V_F}{V_F + V_O} \quad (1)$$

Where V_F, V_O is the free volume, occupied volume of the polymer.[35] Connolly radius was fixed at 1.325 Å.

T_g was obtained from the density-temperature curve in cooling-down simulation from the temperature of 900 K under the isobaric condition.[36]

The dihedral angle between two conjugate planes was identified as the torsion angle. The conformational energies of each torsion angles were calculated with Conformers module.[37] The torsion was set from -180° to 180° with an interval of 1°.

The mean-square radius of gyration (The simulation curve was shown in Figure S1), cohesive energy density (CED) and mean square displacement (MSD) was used to investigate the thermal performance at the scale of the PEIs chains. MSD analysis was conducted to determine the mode of displacement.[38] The MSD could be defined as Eq. (2).

$$\langle r_2(t) \rangle = \frac{1}{N} \sum_{i=1}^{N} \langle |ri(t) - ri(0)| \rangle \quad (2)$$

where $r_i(0)$ and $r_i(t)$ is the initial and final positions of molecules (mass center of particle i) over the time interval t. N is the atom number and brackets denote the ensemble average. Forcite analysis tools were used to calculate the above-mentioned three conformational properties.

DFT calculations were conducted with Dmol3 module to optimize the repeating unit of PEIs and to calculate the electronic performance including dipole moment (μ) and electrostatic precipitator (ESP).

Polarization (α) was calculated with PM3 parameterized model and NDDO approach *via* VAMP module.

3. Results and discussion

3.1. Chemical structure

Infrared spectroscopy was used to characterize chemical structure of polyimide as illustrated in Figure 2. There are four characteristic peaks for polyimide: bending vibration in plane of imide ring at 723-737 cm^{-1}, stretching vibration of C-N on the imide ring at 1370-1378 cm^{-1}, stretching vibration of C=O on the imide ring at 1712-1721 cm^{-1}, asymmetric stretching vibration of C=O on the imide ring at 1771-1780 cm^{-1}. The disappearance of the peak of CO-NH at 1548 cm^{-1} and 1647 cm^{-1} shows the completion of imidization for PI film. And the presence of vibration peak of -CF_3 at 1055 cm^{-1} and 1317 cm^{-1} in Cardo-FAPI are proved that -CF_3 is embedded in the molecular chain. It is also exemplified by the characteristic peak of -O- at 1270-1230 cm^{-1}.

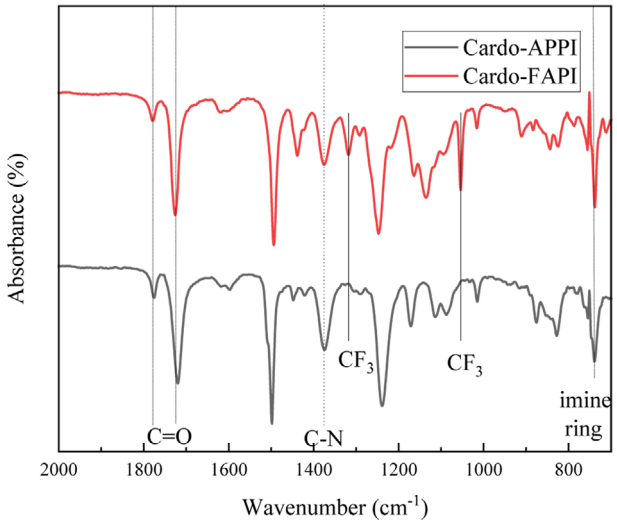

Figure 2. The FT-IR spectra of the PEIs.

3.2. Aggregation structure

WAXD can be used to characterize the degree of order for polymer chains as depicted in Figure 3. As is shown a broad dispersion peak could be found for both polyimides, indicating they are amorphous polymers. The *d*-spacing parameter can be calculated with the peak value of the curve by Bragg Equation $2d\sin\theta = n\lambda$. As calculated the *d*-spacing for Cardo-APPI and Cardo-FAPI is 0.45 nm and 0.51 nm respectively. The introduction of -CF_3 group would increase the *d*-spacing and result in larger FFV in spite of the larger side group Cardo.

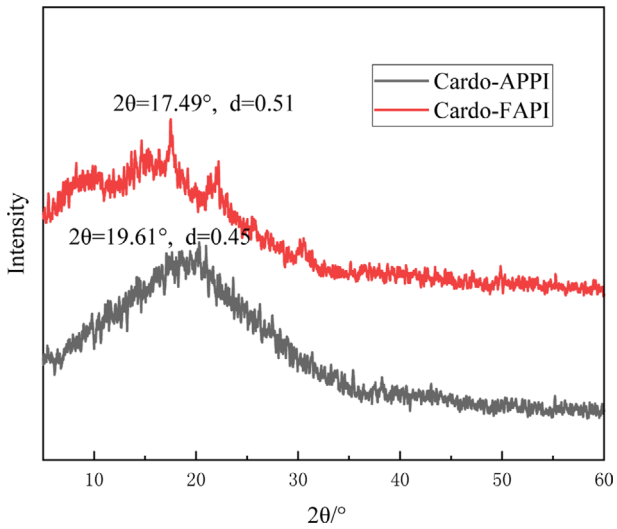

Figure 3. The WAXD profiles of the PEIs.

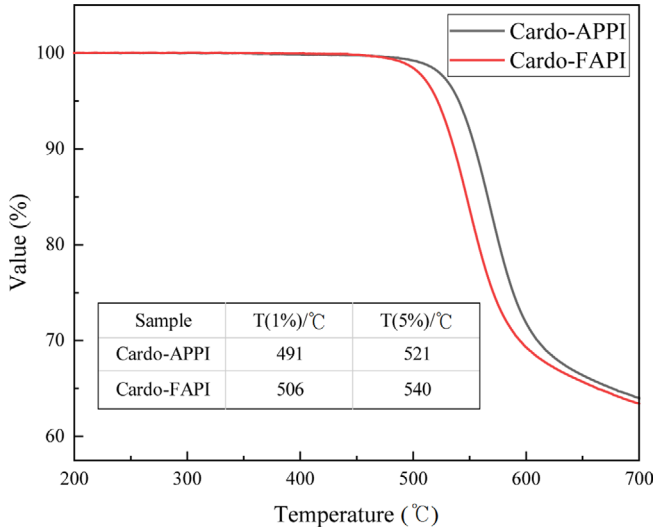

Figure 4. TG curves of the PEIs.

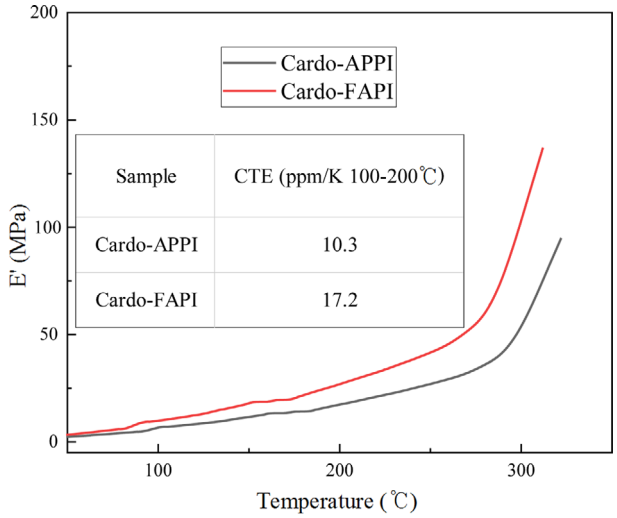

Figure 6. TMA curves of PEIs.

3.3. Thermal properties

The thermal stability of films was evaluated by TGA in Nitrogen atmosphere, as illustrated in Figure 4. Few mass losses could be observed before 300 ℃ and the carbon residue rate exceed 60% at 700 ℃. The thermal decomposition temperature for 1% mass loss remained at 491 ℃ and 506 ℃ respectively, indicating excellent thermal stability. As is shown the heat resistance of Cardo-APPI is superior to that of Cardo-FAPI, proving that the introduction of -CF_3 have an effect on the heat resistance. The bond energy of C-F in trifluoromethyl is lower than that of C-N in imide ring, and the C-F is easy to decompose.

Figure 5 shows the DMA curves as a function of temperature for PEIs at the heating rate of 5 ℃/min. As is depicted the glass transition temperature of Cardo-APPI and Cardo-FAPI is 329 ℃ and 311 ℃ respectively. The addition of -CF_3 increases the free volume and improves the flexibility of polymer chains.

The coefficient of thermal expansion (CTE) was evaluated by TMA curves in Figure 6. The CTE of Cardo-FAPI within 100-200 ℃ is relatively larger for the increase in FFV and mobility of polymer chains. Thermal expansion occurred dramatically at around the glass transition temperature, where the segmental motion speeded up and the film expanded.

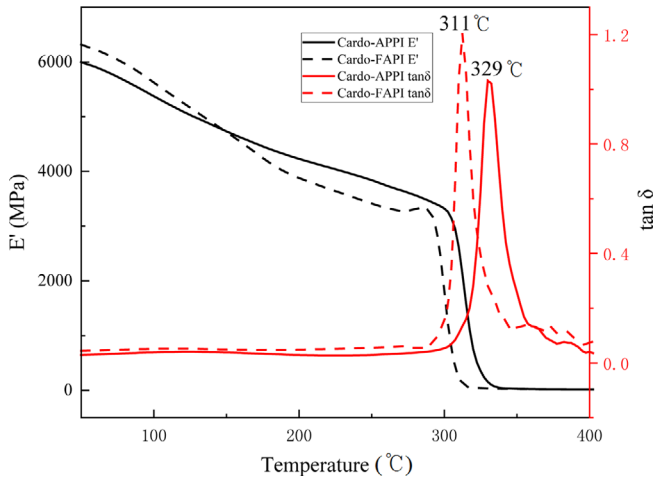

Figure 5. DMA curves of PEIs.

3.4. Molecular simulation

To measure the flexibility of polymer chains the variation of torsion angle and energy of single bond in polymer structural unit was calculated, as displayed in Figure 7. The conformational energy is calculated with the molecular dynamic module in Materials Studio program and it reflect the primary barrier when the single bond rotated. The symbol Ψ1, Ψ2 and Ψ3 represents the torsion angle of C-C-O-C in Cardo diamine, C-O-C-C in Cardo diamine and C-C-N-C connected with Cardo diamine respectively. As is shown in Figure 7, two repeat unit Ψ1 can't rotate for the limited rotation angle on account of large side group Cardo which hinders the movement of chain segments. Ψ1 in Cardo-FAPI is smaller than that in Cardo-APPI for the size effect of -CF_3. While Ψ2 in Cardo-APPI can rotate freely and the rotational barrier remains about 20 kcal/mol. However, the presence of -CF_3 makes the torsion angle can't rotate freely and formed between two benzene rings cannot be coplanar. The flexibility of polymer chains reduces and the ability to change molecular conformation weakens. Trifluoromethyl restricts the rotation of single bond and increases the free volume fraction. As a result of -CF_3 both Ψ3 and torsion barrier in Cardo-FAPI is superior to those in Cardo-APPI.

To investigate the dielectric and optical properties of the polymer electrostatic potential energy and charge transfer distribution of structural unit was simulated by Material studio as illustrated in Figure 8 and the dipole moment and polarizability of the structural unit was also calculated as listed in Table 1.

$$\frac{\varepsilon-1}{\varepsilon+2}=\frac{4\pi}{3}N\left(\alpha_e+\frac{\mu^2}{3k_bT}\right) \quad (3)$$

ε is the dielectric constant, k_b is the Boltzmann constant, T is the temperature, N is the number of polarized molecules per unit, α_e is electric polarizability, and μ dipole moment.

The negative charge on -CF_3 reduces the electron cloud den-

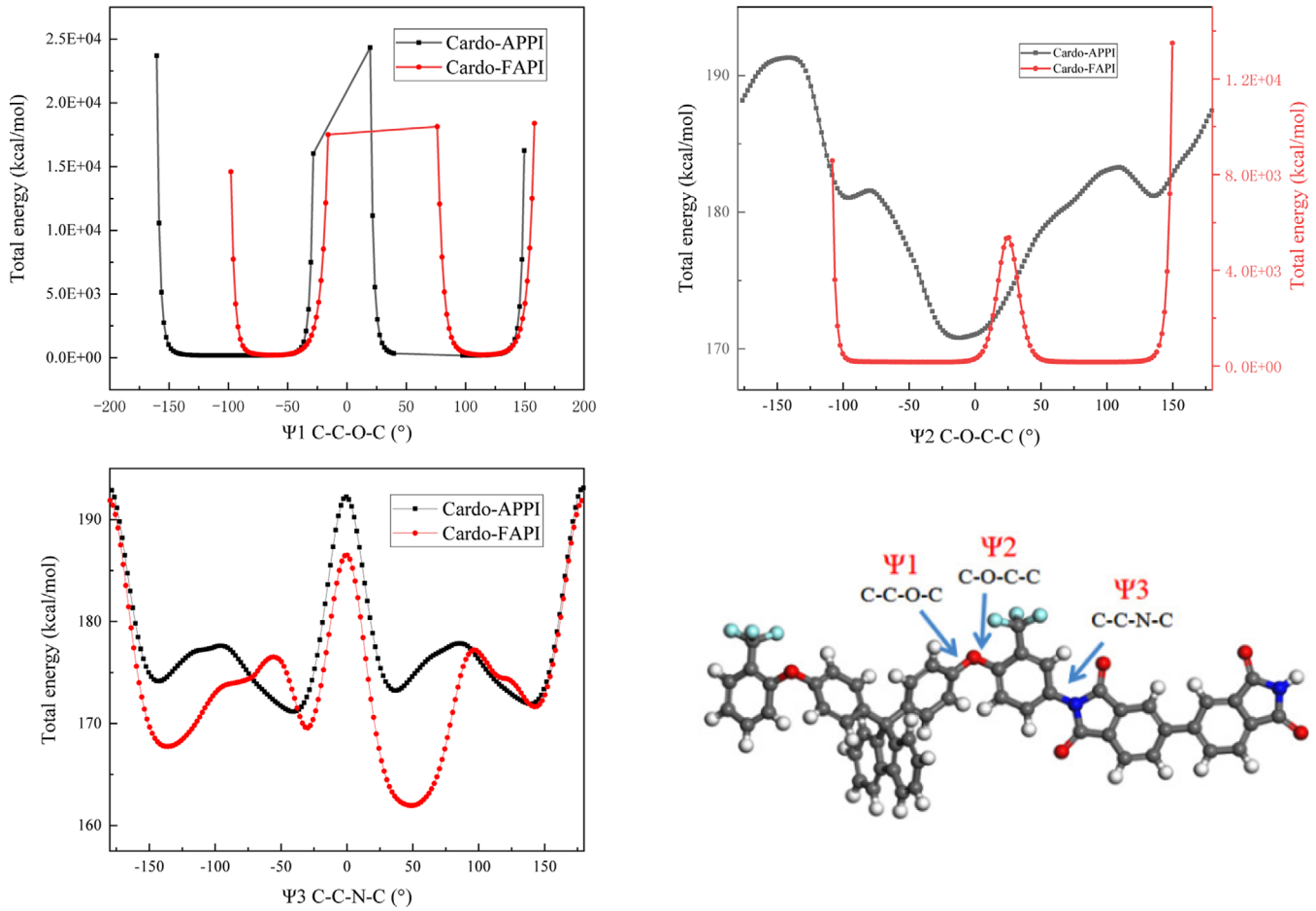

Figure 7. The energy changes in bond rotation of different structural units.

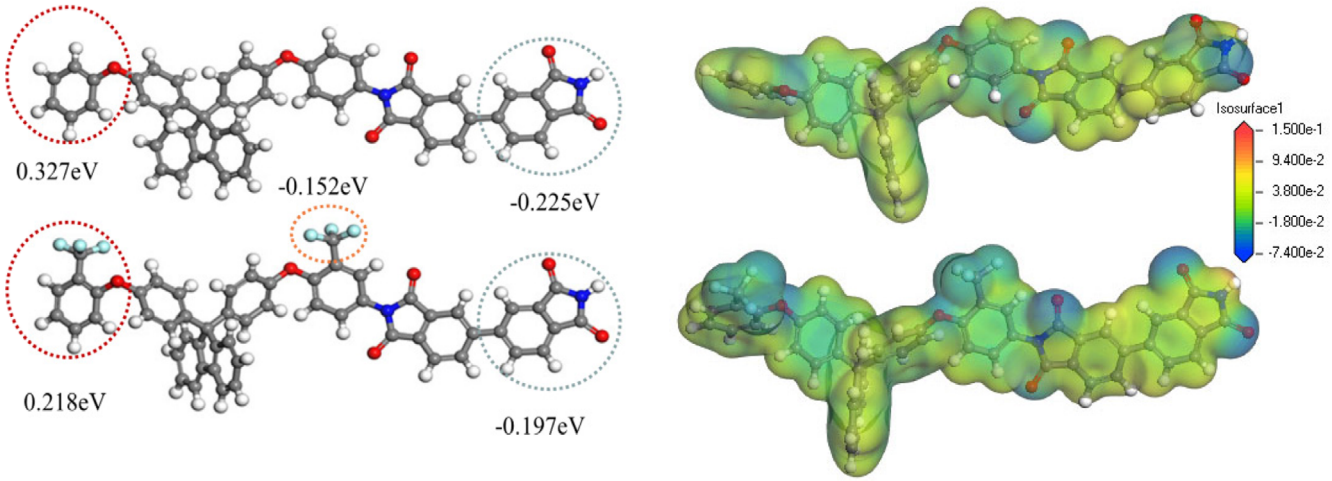

Figure 8. Electrostatic potential energy and charge transfer distribution of structural unit by MS.

Table 1. Dipole moment and polarizability of structural unit by MS

Sample	Dipole moment μ					$V_{vdw}10^{-23}cm^3$	μ/V_{vdw}	α/V_{vdw}
	X	Y	Z	Total	α			
Cardo-PI	-0.092	-0.291	-0.847	1.21	687.74	583.591	0.0020	1.178
Cardo-APPI	-0.049	-1.197	0.775	1.42	881.72	787.353	0.0018	1.120
Cardo-FAPI	0.247	-1.788	1.097	1.51	917.06	889.391	0.0017	1.031

sity on benzene ring and restrains the free delocalization of π electrons on benzene ring, resulting in reduction in polarization of benzene ring in electric field. A charge transfer phenomenon could be observed within structural unit which could increase the transparency and reduce the yellowness. However, it would go against the homogenization of charge density, and would promote the generation of positive and negative charge center within molecules. As could be seen, the electron withdrawing effect of phenoxy and trifluoromethyl resulted in the group being the negative charge center, two negative charge centers are formed near Cardo group as a result of the introduction of $-CF_3$ into structural unit. It would decrease charge transfer from BPDA and increase the transparency of the polymer. It could be concluded from Table 2 that the dipole moment of Cardo-PI, Cardo-APPI, Cardo-FAPI is 0.9, 1.42, and 1.51 respectively in a gradually increasing manner because of the increasing in negative charge center. The dipole moment per unit volume declines dramatically as the addition of phenoxy. Therefore, the introduction of phenoxy and $-CF_3$ increase the free volume and decrease unit dipole moment as well as polarizability, rather than declined the dipole moment and polarization of molecular themselves.

In molecular simulations Lennard-Jones and Coulomb's law is used to describe Van der Waals and electrostatic interaction between polymer chains respectively. CED is used to evaluate the magnitude of intermolecular forces. Table 2 gives the conformational properties of PEIs calculated by Material Studio. As is shown, Van der Waals interaction plays a leading role in the molecular interactions for the four systems. The introduction of ether bond could greatly improve the flexibility of polymer chains, decrease the intermolecular force, and increase the FFV as illustrated in Figure 9. As is revealed by Table 2 the $-CF_3$ group could enhance the FFV of the polymer and decrease the CED, resulting in a decreased density of Cardo-FAPI compared with that of Cardo-PI. Figure S2 shows the simulation Density of PEIs by MS. The larger density of Cardo-FAPI is determined mainly by the grater relative molecular weight of fluorine, and agrees with the calculations by Material Studio.

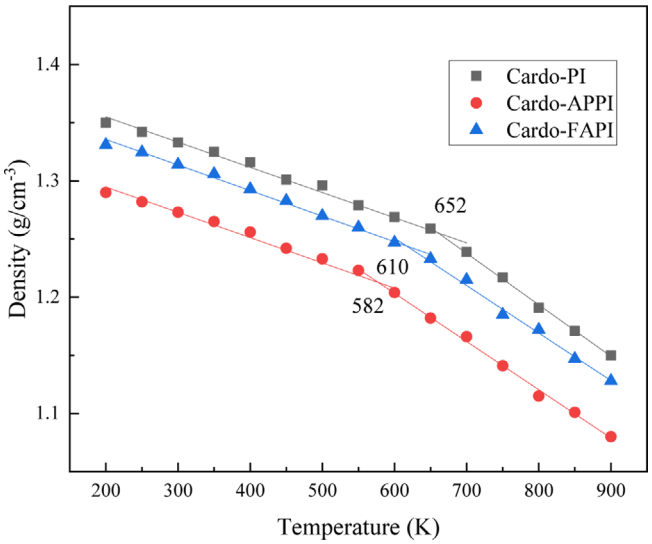

Figure 10. The density-temperature relations of modeled PEIs system by MS.

Figure 10 shows the simulation of the glass transition temperature of PEIs. As revealed the linear fitting inflection point of glass transition temperature is 337 ℃ and 309 ℃ for Cardo-APPI and Cardo-FAPI respectively. Compared with Figure 5 the glass transition temperature obtained from DMA experiments agreed well with those obtained from calculations, indicating high accuracy of simulation data.[39] The glass transition temperature of Cardo-PI is calculated to be 379 ℃, which is not available to detect experimentally for its brittleness.

The static parameters of PEIs chains are listed in Table 2. MSD is calculated from the path of MD and used to investigate the dynamic migration rate of PI chains, as is shown in Figure 11.

Table 2. Conformational properties of PEIs by MS

Sample	S2	FFV (%)	CED (10^8J·cm^{-3})	Van der Waals (10^8J·cm^{-3})	Electrostatic (10^8J·cm^{-3})	Density (g/cm^3)	Simulated density (g/cm^3)
Cardo-PI	23.5	28	3.39	2.87	0.52	-	1.34
Cardo-APPI	28.2	32	3.23	2.65	0.46	1.31	1.28
Cardo-FAPI	33	37	3.05	2.31	0.33	1.35	1.32

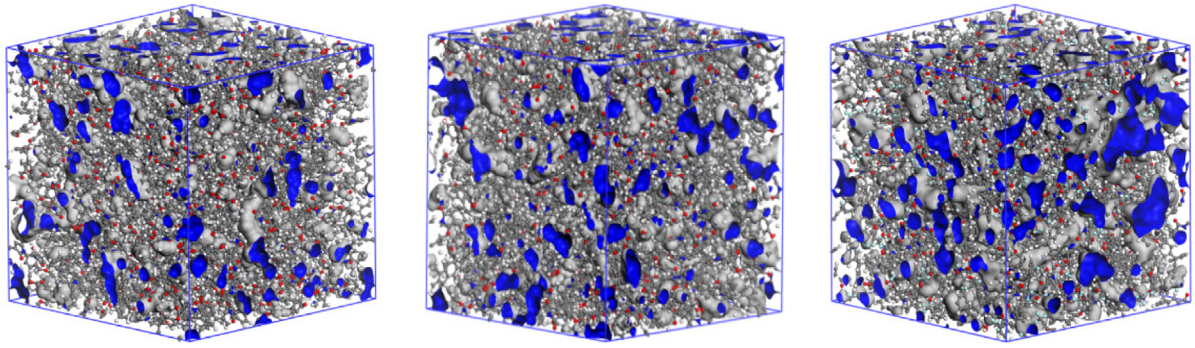

Figure 9. Free volume topography image of PEIs by MS.

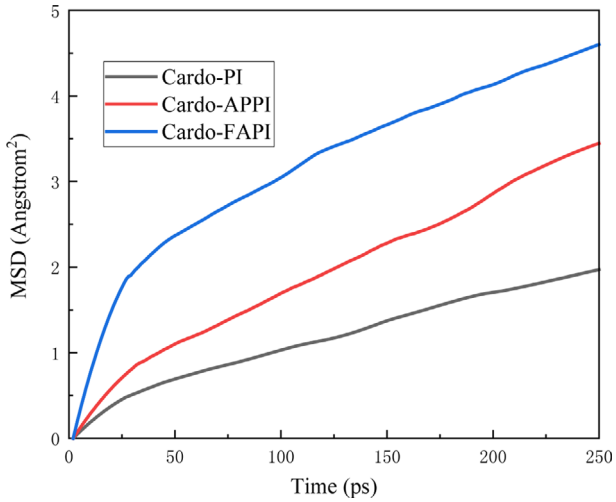

Figure 11. MSD of different PEIs by MS.

The slope of MSD curve represents the migration rate of polymer chains. The freely rotational ether bond in Cardo-APPI increase the flexibility of polymer chains and lower the glass transition temperature. The introduction of difficult to rotate -CF_3 group into Cardo-FAPI could result in rotational troubles for torsion angle and higher migration rate because of the increased FFV.

3.5. Dielectric properties

Figure 12 gives the variation of relative dielectric constant and dielectric loss of PEI films within the available scope of frequency. As is shown, the dielectric constant of the film decreases while the dielectric loss increases with the frequency more than 10 MHz. At lower frequency polymer chains segment of small size would be polarized but the dielectric loss is not sensitive to the variation of frequency and remain at lower level. While in the higher alternating electric field the polarization of polyimide chain segments is enhanced and the speed of polarization fell behind that of electric field direction. The hysteresis of chain polarization result in an increase in dissipation, and cause a decline of dielectric constant and an increase in dielectric loss.[40] At the frequency of 1 MHz the dielectric constant of both PEI is lower than 3 for the existence of larger Cardo side group. The dielectric constant of Cardo-FAPI decrease from 2.91 to 2.83 when the -CF_3 group is introduced. Both lower electronic polarizability and molecular bulk density cause by -CF_3 contributed to the reduction of dielectric constant of Cardo-FAPI.

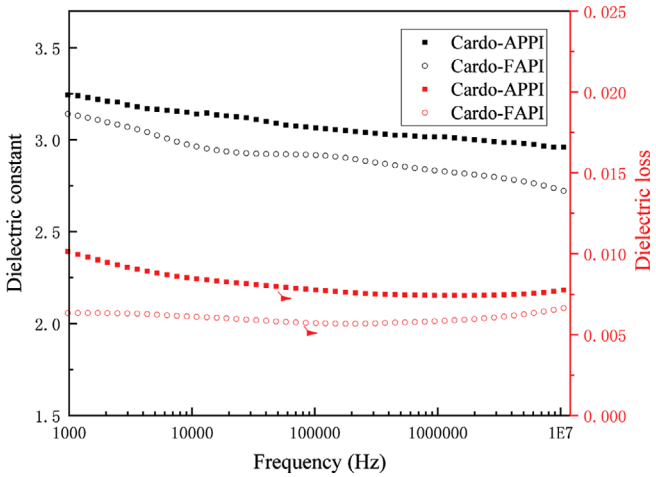

Figure 12. Dielectric constant and dielectric loss of PEIs.

3.6. Optical properties

Figure 13 displays the optical properties of PEIs with UV-vis. As is revealed the transmittance of both polymers reach 87% at the wavelength of 450 nm, and the cut-off wavelength (λ_0) for Cardo-FAPI and Cardo-APPI remain 360 nm and 380 nm respectively. The noncoplanar structure of Ψ1 in C-C-O-C and larger side group in the two kinds of polymer increase the chain gaps and free volume, weakened the interaction force between molecular chains, and restrained the charge transfer and formation of CTC, which would result in higher transmittance.

Compared with Cardo-APPI, the -CF_3 group in Cardo-FAPI increase the d-spacing and decrease the bulk density as well as the interaction force between molecular chains, which would prevent the formation of CTC. High electronegativity for fluorine could destroy the conjugation of electron cloud in micromolecular level and reduce the possibility to form CTC. Therefore, the absorbable wavelength for polyimide could shift leftward and make it not absorb visible spectroscopy. Thus, polyimide with excellent transmittance could be obtained.

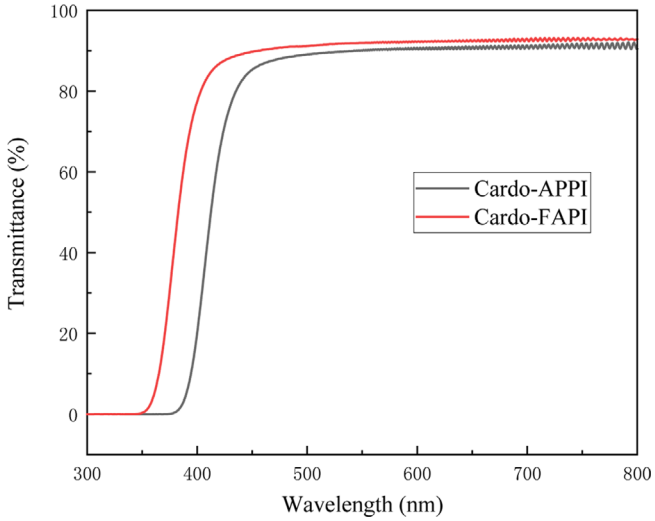

Figure 13. UV-vis transmission spectra of the PI films.

Table 3. The mechanical properties of PEIs

Sample	Inherent viscosity (pa·s)	Strength (MPa)	Modulus (GPa)	Elongation (%)
Cardo-APPI	102	222 ± 18	6.3 ± 1.2	22 ± 5
Cardo-FAPI	98	184 ± 22	6.9 ± 0.9	16 ± 6

Table 4. Solubility of PEIs[a]

Sample	DMF	DMAc	NMP	DMSO	Py	*m*-Cresol	Dioxane	THF
Cardo-APPI	-	-	-	-	-	-	-	-
Cardo-FAPI	+	+	+	+	+	+	+	+

[a]Qualitative solubility testing: 10 mg of PEIs in 1 mL of solvent for 24 h: +, soluble at room temperature; -, insoluble. DMF: N,N-dimethylformamide; DMAc: *N*,*N*-dimethylacetamide; NMP: *N*-methyl-2-pyrrolidone; DMSO: dimethyl sulfoxide; Py: pyridine; THF: tetrahydrofuran.

3.7. Mechanical and soluble properties

The mechanical performance of PI film is listed in Table 3. The viscosity of Cardo-APPI and Cardo-FAPI remained 450 ± 10 pa·s and 300 ± 10 pa·s respectively when the amount of dianhydride reached 100%. The trifluoromethyl attached to benzene ring has a strong electronic absorption ability, which will result in the reduction of the electron-donating ability for the amino group in Cardo-FA. Therefore, the molecular weights of PAA prepared with Cardo-FA are lower than that of PAA with Cardo-AP as a result of the lower reaction activity for Cardo-FA. The viscosity of the PAAs were set to be 100 ± 10 pa·s for convenience of comparison. Both the tensile strength and elongation at break of Cardo-APPI was superior to that of Cardo-FAPI in this study.

The introduction of trifluoromethyl as pendant group increases the free volume fraction and d-spacing and leads to lower tensile strength. The restriction of charge transfer effect would cause lower intermolecular force between molecular chains and decrease the mechanical performance.

The solubility of PEIs was tested in various solvents and the results were displayed in Table 4.

Cardo-FAPI has excellent solubility in both aprotic polar solvents (NMP, DMAc, DMF, and DMSO) and non-aprotic solvent (m-cresol, pyridine, and dioxane). Compared with Cardo-APPI, Cardo-FAPI show better solubility. The good solubility of Cardo-FAPI might be due to the presence of -CF_3 groups, which would increase the d-spacing and decrease the interaction between molecular chains. The solution molecules could easily penetrate into the polymer chains, leading to a reduction in viscosity.

4. Conclusions

PEI containing two kinds of Cardo group was prepared and the representative properties was investigated. The results showed that the introduction of -CF_3 had significant effect on the microstructure and performance of polyimide. The cut-off wavelength of polyimide containing -CF_3 decreased from 380 nm to 360 nm and the dielectric constant decreased from 2.91 to 2.83. The molecular simulation results showed that -CF_3 could restrain the charge transfer and improve the transmittance of polyimide film. The larger size -CF_3 increased the FFV and lowered the CED and T_g of polyimide film. The insight obtained from this paper can offer valuable references to the synthesis and optimization of processing technique to obtain PEI of lower dielectric constant and higher transparency containing Cardo group.

Supporting information: Information is available regarding the molecular simulation results for the polymer and characterization of diamine. The materials are available *via* the Internet at http://www.springer.com/13233.

References

(1) M. Jia, Y. Li, C. He, and X. Huang, *ACS Appl. Mater. Interfaces*, **8**, 26352 (2016).
(2) Y. Zhuang, R. Orita, E. Fujiwara, Y. Zhang, and S. Ando, *Macromolecules*, **52**, 3813 (2019).
(3) M. Hasegawa and K. Horie, *Prog. Polym. Sci.*, **26**, 259 (2001).
(4) P. K. Tapaswi and C. Ha, *Macromol. Chem. Phys.*, **220**, 1800313 (2019).
(5) D. J. Liaw, K. L. Wang, Y. C. Huang, K. R. Lee, J. Y. Lai, and C. S. Ha, *Prog. Polym. Sci.*, **37**, 907 (2012).
(6) Y. Qiao, X. Yin, T. Zhu, H. Li, and C. Tang, *Prog. Polym. Sci.*, **80**, 153 (2018).
(7) H. Wang, X. Ji, Z. Li, and F. Huang, *Adv. Mater.*, **29**, 1606117 (2017).
(8) V. V. Korshak, S. V. Vinogradova, and Y. S. Vygodskii, *J. Macromol. Sci. Part C Polym. Rev.*, **C11**, 45 (2008).
(9) C. Yang, Y. Su, and M. Hsu, *Polym. Int.*, **56**, 415 (2010).
(10) L. Yi, C. Li, W. Huang, and D. Yan, *J. Polym. Sci. Part A Polym. Chem.*, **54**, 976 (2016).
(11) C. Wang, X. Zhao, G. Li, and J. Jiang, *Polym. Degrad. Stab.*, **94**, 1746 (2009).
(12) X. Ma, O. Salinas, E. Litwiller, and I. Pinnau, *Macromolecules*, **46**, 9618 (2013).
(13) Rimpa, Chatterjee, Sipra, Ghosh, Soumendu, Bisoi, Susanta and Banerjee, *J. Appl. Polym. Sci.*, **134**, 45213 (2017).
(14) J. Fang, X. Guo, S. Harada, T. Watari, K. Tanaka, H. Kita, and K. I. Okamoto, *Macromolecules*, **35**, 9022 (2002).
(15) P. Wen, Y. Kim, H. Chun, S. Y. Yang, and M. H. Lee, *Mater. Chem. Phys.*, **139**, 923 (2013).
(16) M. Hasegawa, S. Takahashi, S. Tsukuda, T. Hirai, J. Ishii, Y. Yamashina, and Y. Kawamura, *Polymer*, **169**, 167 (2019).
(17) S. J. Zhang, Q. Q. Bu, Y. F. Li, C. L. Gong, X. Y. Xu, and H. Li, *Mater. Chem. Phys.*, **128**, 392 (2011).
(18) L. Qu, S. Huang, Y. Zhang, Z. Chi, S. Liu, X. Chen, and J. Xu, *J. Mater. Chem. C*, **5**, 6457 (2017).
(19) S. Xu, M. Yang, and S. Cao, *React. Funct. Polym.*, **66**, 471 (2006).
(20) Y. W. Liu, L. S. Tang, L. J. Qu, S. W. Liu, Z. G. Chi, Y. Zhang, J. R. Xu, P. Lab, and G. H. Lab, *Chinese J. Polym. Sci.*, **37**, 13 (2019).
(21) J. Q. Lin, H. Lin, W. L. Yang, X. K. Li, Y. Liu, Z. B. Xie, and P. N. Zhang, *Adv. Mater. Res.*, **785**, 556 (2013).
(22) X. Wang, H. Wang, L. Luo, J. Huang, J. Gao, and X. Liu, *RSC Adv.*, **2**, 9463 (2012).
(23) M. Zhang, C. Liu, J. Yang, P. Yang, L. Zhang, and J. Dong, *J. Proteomics*, **159**, 47 (2017).
(24) N. Taniguchi, Y. Abe, Y. Mitooka, and T. Kitagawa, *Eur. Polym. J.*, **88**, 9 (2017).
(25) V. M. Nazarychev, A. V. Lyulin, S. V. Larin, I. V. Gofman, and S. V. Lyulin, *Macromolecules*, **49**, 6700 (2016).
(26) Y. Wang, Y. Yang, Z. Jia, J. Qin, and G. Yi, *Polymer*, **53**, 4157 (2012).
(27) K. Cho, D. Lee, S. L. Min, and E. P. Chan, *Polymer*, **38**, 1615 (1997).
(28) Rimpa, Chatterjee, Sipra, Ghosh, Soumendu, Bisoi, Susanta, and Banerjee, *J. Appl. Polym. Sci.*, **134**, 45213 (2017).
(29) C. P. Yang and J. H. Lin, *J. Polym. Sci. Part A: Polym. Chem.*, **31**, 2153

(1993).
(30) Y. Shu, D. Wang, F. Bo, N. Liu, Y. Lu, J. Huo, Y. Yong, B. Peng, X. Ding, and Y. Shu, *Comp. Mater. Sci.*, **152**, 158 (2018).
(31) G. Marque, S. Neyertz, J. Verdu, V. Prunier, and D. Brown, *Macromolecules*, **41**, 498 (2008).
(32) D. Bera, P. Bandyopadhyay, S. Ghosh, S. Banerjee, and V. Padmanabhan, *J. Membr. Sci.*, **474**, 20 (2015).
(33) S. Seethamraju, P. C. Ramamurthy, and G. Madras, *ACS Appl. Mater. Interfaces*, **5**, 4409 (2013).
(34) B. T. Low, Y. Xiao, and S. C. Tai, *Polymer*, **50**, 3250 (2009).
(35) Y. W. Liu, J. Huang, J. H. Tan, Y. Zeng, Q. Ding, X. W. Xiang, Y. J. Liu, and H. L. Zhang, *J. Polym. Sci. Part A: Polym. Chem.*, **55**, 2373 (2017).
(36) H. Lei, S. Qi, and D. Wu, *Polymer*, **179**, 121645 (2019).
(37) S. V. Glu, N. Mga, and S. U. Tantekin-Ersolmaz, *J. Membr. Sci.*, **417**, 217 (2012).
(38) K. S. Chang, Z. C. Wu, S. Kim, K. L. Tung, Y. M. Lee, Y. F. Lin, and J. Y. Lai, *J. Membr. Sci.*, **454**, 1 (2014).
(39) C. K. Min, T. B. Wu, W. T. Yang, and C. L. Chen, *Compos. Sci. Technol.*, **68**, 1570 (2008).
(40) S. Han, Y. Li, F. Hao, H. Zhou, and D. Wu, *Eur. Polym. J.*, **143**, 110206 (2020).

